

Microstructure and Electrical Characterization of Thermoelectric Nanocrystalline Bi₂Te₃ Synthesized by Mechanical Alloying

Saikat Kumar Kantar^a, Shrabani Paul^a, Tuli Chatterjee^b, Hema Dutta^c, Swapan Kumar Pradhan^{a*}

^aMaterials Science Division, Department of Physics, The University of Burdwan, Golapbag, Burdwan 713104, West Bengal, India

^bDepartment of Physics, National Institute of Technology, Durgapur, West Bengal, India

^cDepartment of Physics, Vivekananda College, Burdwan 713103, West Bengal, India

Received: May 08, 2019; Accepted: August 05, 2019

Nanocrystalline bismuth telluride, Bi₂Te₃ has been synthesized by mechanical alloying (MA) the powder mixture composed of Bi and Te in the inert gas atmosphere within a short duration of 15 min. Microstructure characterization of the prepared powder has been investigated adopting the Rietveld's method using X-Ray diffraction (XRD) data and analyzing high-resolution transmission electron microscopy (HRTEM) images. The XRD pattern of 15 min milled powder is composed of reflections of major Bi₂Te₃ phase with other two minor phases. Detailed structural information of these minor phases has been reported here which was not explored in any previous works. XRD analysis reveals that the stoichiometric Bi₂Te₃ phase has been formed after 1h of milling and there is no phase transition up to 10h of milling. HRTEM study also reveals the formation of single phase nanostructured Bi₂Te₃ phase. The DC (direct current) conductivities of 15min, 30min and 10h milled powders are measured within the temperature range of 359 to 633K. The electrical conductivity (σ) of Bi₂Te₃ indicates the semiconducting nature of the sample. There is no significant change of electrical conductivity of Bi₂Te₃ phase since its formation after 15min to 10h of milling, as there is no noticeable change in crystallite size.

Keywords: Nanostructured materials, mechanical alloying, microstructure, X-ray diffraction, HRTEM.

1. Introduction

As fossil fuel resources are becoming exhausted, thermoelectric (TE) devices, as alternative power resources have found their applications in power generators or cooling devices^{1,2}. Currently, due to relatively low efficiency and high cost, TE materials have limited applications. TE materials can play a vital role in energy conservation if efficient and stable novel materials can be prepared in a cost-effective way. Bismuth telluride based alloys are well known potential TE materials for near room temperature applications due to their low thermal conductivity and large Seebeck coefficient³⁻⁵. Reducing the crystallite size of polycrystalline TE materials to the nano-scale has resulted in a significant reduction of the lattice thermal conductivity and improvement in the figure of merit^{6,7}. Most of these advances are related to the use of nanostructures due to thermal conductivity reduction^{8,9}. Alternatively, composite TE materials containing several phases may have higher efficiency introducing more interfaces leading to a decrease in the thermal conductivity. The aim of the present research work is the production of nanostructured bismuth telluride thermoelectric material in a low-cost method. For this purpose, we have employed the MA method to prepare nanocrystalline bismuth telluride alloy starting from an elemental powder mixture of Bi and Te at room temperature.

This simple and cost-effective preparation route has the advantage to produce nano-dimensional Bi₂Te₃ powder in large quantities in a very short duration of time. Although several reports on mechanosynthesis of single/composite TE materials have been published¹⁰⁻¹⁴, the growth mechanism of bismuth telluride TE material synthesized by mechanical alloying (which may lead to the formation of nanocomposites including several constituent phases of the same family), has not been reported yet. Earlier review shows that during growth process Bi₂Te₃ may co-exist with different high-pressure phases, which are still remained unidentified so far the structure report is concerned^{15,16}. In another work, synthesis of Bi₂Te₃ was prepared by mechanical milling in a short time but the appearance of other phases in the XRD pattern was ignored and so the growth mechanism of stoichiometric Bi₂Te₃ phase remains unexplored¹⁷. In the present work, XRD pattern analysis reveals that at relatively lower time milling (15min and 30 min) major rhombohedral Bi₂Te₃ phase has been formed along with a trace amount of two minor phases. Formations of such intermediate metastable high-pressure phases during mechanical alloying were already reported by ourselves^{18,19}. However, higher time of milling after 1h produces single phase nanocrystalline Bi₂Te₃, which remains stable up to 10h of milling. Detailed structural information of the hitherto unidentified phases evolved in the way of formation Bi₂Te₃ has been reported in the present work.

*e-mail: skpradhan@phys.buruniv.ac.in

In this study, Rietveld's powder structure refinement method has been adopted to analyze the XRD data²⁰⁻²⁴ for microstructure characterization and phase quantification of the individual phases in the unmilled powder mixture and all ball-milled powder samples. The Rietveld method was successfully applied for phase quantification and microstructure characterization measuring lattice imperfections of several multiphase materials²⁵⁻²⁷. Microstructure characterization and phase identification of the 10h milled powder have also been carried out by analyzing HRTEM images. The DC electric conductivities of 15min, 30min and 10h ball-milled samples are measured within the temperature range of 359 to 633K to validate the semiconducting nature of the prepared materials.

The general objective of the present work is to search for a cost and time efficient technique to synthesize nanostructured Bi₂Te₃ TE material, with the possibility of commercialization and mass production of the material. Besides this, explanation of growth mechanism by exploring the structure of metastable phases evolved in the early stage of milling, which would advance the knowledge in the field of production of TE nanocomposites as well as their contribution to the thermoelectric power. The specific objectives of this work are to study the structure/microstructure and phase quantification of bismuth telluride based composites in the way of formation single phase Bi₂Te₃ compound and their electrical characterization. It is expected that the reduction of crystallite size of Bi₂Te₃ down to nano-dimension effectively reduces the lattice thermal conductivity and increases electrical conductivity, which in turn improves the thermoelectric performance of nanocrystalline Bi₂Te₃.

2. Experimental

MA was performed at room temperature using a high-energy planetary ball mill (Model-P6, M/s FRITSCHE, GmbH, Germany). Starting elements pure Bi (M/s Loba Chemie; purity 99.5%) and Te (M/s Sigma Aldrich; purity 99.5%) powders were mixed in 2:3 molar ratio. The powder mixture was kept in a chrome steel vial (80 ml volume) with 30 numbers of chrome steel balls (10 mm size) sealed in a glove box under flowing Ar atmosphere. The ball-to-powder mass ratio (BPMR) was 40:1. Milling was paused after a selected time interval (15min after every 15min of milling) and milled powders were collected from the vial. XRD data of unmilled and all ball milled powder samples were collected from an X-ray powder diffractometer (Bruker; Model D8 Advance Da Vinci) operated at 40 kV and 40 mA with Ni-filtered CuK_α radiation in step-scan mode (step size 0.02° 2θ and counting time 30s/step) within the angular range of 20°-80° 2θ. For HRTEM study, the 10h ball milled powder was finely dispersed in alcohol using ultrasonic vibrator and then a tiny drop of the solution placed on a 300 mesh carbon-coated Cu-grid. The HRTEM was operated at 200KV (Model HR-TEM, JEOL JEM 2100) to obtain well-resolved HRTEM micrographs of nanocrystalline Bi₂Te₃ particles.

The DC electrical conductivities of 15min, 30min and 10h ball-milled samples were measured by a standard four-probe method using 8 1/2-digit Agilent 3458 multimeter and 6514 Keithley Electrometer. To measure the DC conductivity, pellets of 1cm diameter was prepared by pressing the powder mixture under a hydraulic press at 500 MPa. Silver paint was used to fix the fine copper wires (probes) on both surfaces of the pellets.

3. Microstructure Evolution by X-ray Diffraction

Microstructure characterization of the materials under study has been revealed employing the Rietveld's whole profile fitting method. The Rietveld software, MAUD 2.79²⁰ has been successfully employed for the entire analysis. Powder XRD patterns are simulated incorporating structural and microstructural parameters of following individual phases (i) Bi (trigonal, S.G.: R-3m:H, $a = 0.4547$ nm, $c = 1.1861$ nm) (ii) Te (trigonal, S.G.: P3121, $a = 0.4459$ nm, $c = 0.5927$ nm) (iii) Bi₂Te₃ (trigonal, S.G.: R-3m:H, $a = 0.4423$ nm, $c = 3.0085$ nm), (iv) BiTe (I) (trigonal, S.G.: P-3m1, $a = 0.4386$ nm, $c = 3.0545$ nm), and (v) BiTe (II). (trigonal, S.G.: P-3m1, $a = 0.4477$ nm, $c = 1.8719$ nm). XRD step scan data are used to obtain the refined structural and microstructural parameters, such as lattice parameters, crystallite size and r.m.s. lattice strain.

Refinement minimizes the difference between the observed experimental and simulated powder diffraction patterns and continues until convergence is reached. Value of the quality factor Goodness of fitting (GoF~1) confirms the goodness of refinement²¹⁻²⁵:

$$GoF = R_{wp}/R_{exp}$$

where R_{wp} (weighted residual error) and R_{exp} (expected error) are reliability index parameters.²¹⁻²⁵

The Rietveld analysis can explore quantitative phase abundances of the composite materials²⁶⁻³⁰ and also has been adopted for precise phase quantification of ball-milled Bi-Te powder mixture in the present study.

4. Results and Discussion

4.1 Microstructure characterization by XRD and HRTEM study

Fig. 1 represents the XRD patterns of unmilled (0h) and all ball-milled (15min-10 h) Bi-Te powder mixture. XRD pattern of unmilled powder mixture (0h) shows none other than reflections of starting Bi (ICSD # 2446663) and Te (ICSD # 161690) phases with intensities in accordance to their respective contents in the mixture powder. Theoretically simulated patterns (I_s) are refined for best fitting with the experimental patterns (I_o) and the final fitted patterns are illustrated in Fig. 1. Almost linear fitting residuals ($I_o - I_s$) are plotted at the bottom of individual patterns.

Nature of fitting residual and value of quality factors of the fitting, GoF (1.01-1.42) simultaneously gives evidence that the experimental patterns have fitted well with theoretically simulated and refined patterns²⁸⁻³⁰.

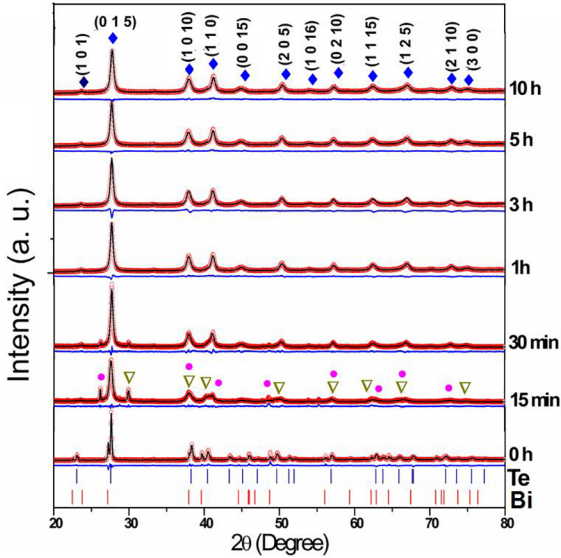


Figure 1. Rietveld output of X-ray powder diffraction patterns of ball-milled Bi-Te powder mixtures. Experimental data points are shown as hollow circles, while refined simulated patterns are shown as continuous lines. The difference between the experimental data (I_e) and the fitted simulated pattern (I_f) is shown as a continuous line under respective diffraction pattern. Presence of BiTe (I) (●) and BiTe (II) (▽) in 15min milled sample is shown with different symbols. The peak positions of Bi and Te are shown as small solid bar markers at the bottom of the figure. Crystal planes of Bi_2Te_3 are indexed in XRD pattern of 10 h ball-milled powder.

Only 15 min of milling results in a significant change in the XRD pattern as evidenced in Fig. 1. Most of the strong reflections of Bi_2Te_3 (ICSD # 158366) phase have been appeared in the pattern with noticeable peak broadening along with two additional reflections around the major (015) reflection of Bi_2Te_3 phase. It is interesting to note that there is no trace of either of the two elemental reflections in the XRD pattern. It clearly reveals that the required Bi_2Te_3 phase has been synthesized within 15min of milling with an insignificant amount of secondary phases. Development of unknown phases during the synthesis of Bi_2Te_3 had been reported in some previous works^{15,16}. We have identified the new structurally unknown phases produced in the relatively lower milling time as BiTe (I) and BiTe (II) (ICSD # 9000678) phases with similar structure but different lattice parameter values (Table 1).

After 30 min of milling, intensities of BiTe phases reduce to a minimum. However, the XRD pattern of 1h ball-milled powder shows only the reflection of Bi_2Te_3 phase, signifying a higher time of milling after 1h produces single phase Bi_2Te_3 . Extended milling upto 10h results only in peak-broadening associated with lowering the crystallite size and increasing r.m.s. strain of mechanically alloyed Bi_2Te_3 powder. Atomic models of BiTe (I), Bi_2Te_3 and BiTe (II) (sequence follows the reflection position of the corresponding phases in the XRD patterns of 15min and 30 min milled powder) phases are represented in Fig. 2 depicting atomic positions of Bi and Te in different structural phases evolved during the milling process.

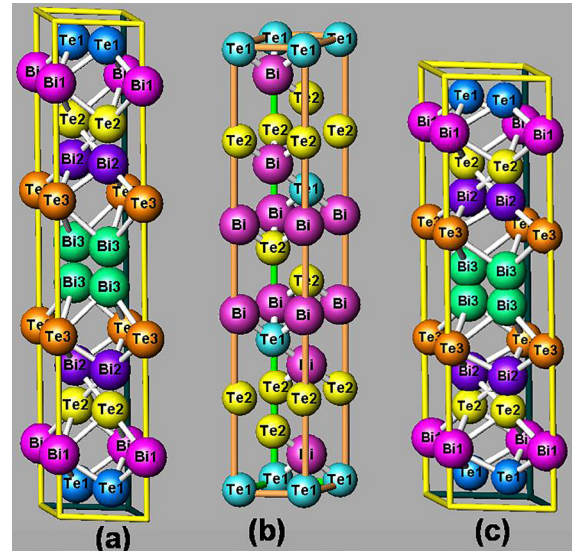


Figure 2. Atomic model of (a) BiTe (I) (b) Bi_2Te_3 and (c) BiTe (II) phases.

Results of the Rietveld analysis are plotted in Figs. 3-5 and tabulated in Table 2 to reveal the phase transformation kinetics and microstructure characterization of Bi-Te powder mixtures. It is to be noted that Bi_2Te_3 phase has been evolved as major phase (~90 mol%) just after 15 min of milling with BiTe (I) (~5.4mol%) and BiTe (II) (~4.6mol%) phases. After 1h of milling, Bi_2Te_3 phase formation has been completed with the disappearance of two minor phases. The detailed microstructure of single phase Bi_2Te_3 has been analyzed by Rietveld refinement and obtained results are plotted in these figures.

The variations of lattice parameters of Bi_2Te_3 with increasing milling time are shown in Fig. 3 and Table 2.

Table 1. Structural information of BiTe (I) and BiTe (II) developed after 15 min of milling.

Phase	Lattice parameters (nm)		Atomic coordinates(z)					
	a	c	Te1	Te2	Te3	Bi1	Bi2	Bi3
BiTe (I)	0.4386	3.0545	0.1015	0.2248	0.3631	0.1252	0.2922	0.4593
BiTe (II)	0.4477	1.8719	0.0744	0.2240	0.3699	0.1293	0.2952	0.4528

It is evident that the lattice parameter 'a' remains the same throughout the milling process, though there is a tendency of a small increase of 'c' lattice parameter with increasing milling time. After 5h of milling, lattice parameter values are saturated and remain unchanged till the final stage of milling of 10 h.

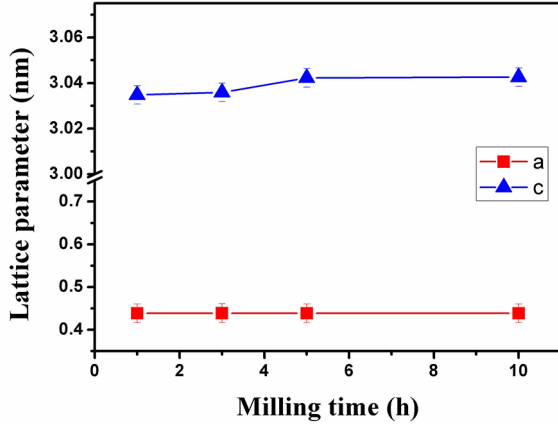


Figure 3. Variation of lattice parameters of Bi_2Te_3 phase with increasing milling time.

After the formation of Bi_2Te_3 phase, both crystallite sizes and lattice strain values are found to be anisotropic in nature. Crystallite sizes are relatively large along $[1\ 1\ 0]$ (~22.5 nm) and $[0\ 1\ 5]$ (~20 nm) with respect to $[1\ 0\ 10]$ (~16 nm) (Fig. 4). In the course of milling, initially crystallite sizes in different crystallographic directions are decreased to a large extent

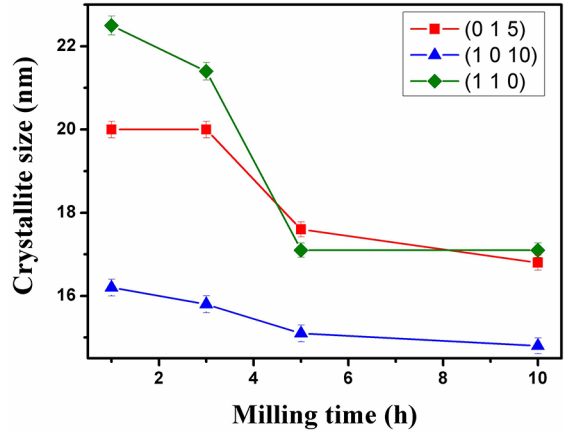


Figure 4. Variation of crystallite sizes of Bi_2Te_3 phase with increasing milling time.

Table 2. Microstructure parameters of unmilled and ball milled Bi_2Te_3 revealed by Rietveld's X-ray powder structure refinement analysis.

Milling time	Phase present	Mol fraction $\pm[10^{-3}$ to $10^{-2}]^*$	Lattice Parameter $\pm[10^{-5}$ to $10^{-3}]^*$			Plane direction	Particle Size (nm) $\pm[10^{-2}$ to $10^{-1}]^*$	R.m.s strain $\langle\langle\epsilon_L^2\rangle\rangle^{1/2} \times 10^3 \pm[10^{-3}$ to $10^{-2}]^*$
			a (nm)	b (nm)	c (nm)			
0 min	Bi	0.100	0.4547	0.4547	1.1861		125.7	0.025
	Te	0.900	0.4459	0.4459	0.5927	(100)	104.1	2.74
15 min	Bi_2Te_3	0.875	0.4426	0.4426	3.0256	(015)	22.3	0.30
	BiTe (I)	0.060	0.4386	0.4386	3.05451.8719	(1 0 10)	16.2	0.60
	BiTe (II)	0.065	0.4477	0.4477		(1 1 0)	22.8	1.16
30 min	Bi_2Te_3	0.969	0.4394	0.4394	3.0292	(015)	34.0	1.92
	BiTe (I)	0.014	4.3824	4.3824	3.0546	(1 0 10)	40.2	1.73
	BiTe (II)	0.017	4.4369	4.4369	1.8945	(1 1 0)	20.7	1.30
							16.5	1.50
							22.3	2.20
1h	Bi_2Te_3	1	0.4386	0.4386	3.0348	(015)	18.6	2.17
						(1 0 10)	21.3	2.39
						(1 1 0)	20.0	1.65
3h	Bi_2Te_3	1	0.4389	0.4389	3.0359	(015)	16.2	3.55
						(1 0 10)	22.5	3.22
						(1 1 0)	16.2	0.60
5h	Bi_2Te_3	1	0.4387	0.4387	3.0423	(015)	20.0	1.62
						(1 0 10)	15.8	3.63
						(1 1 0)	21.4	3.23
10h	Bi_2Te_3	1	0.4386	0.4386	3.0426	(015)	17.6	1.89
						(1 0 10)	15.1	4.58
						(1 1 0)	17.1	2.11
						(015)	16.8	2.31
						(1 0 10)	14.8	4.68
						(1 1 0)	17.1	2.50

with increasing milling time and then approached towards saturation values. In general, though the nature of variations is different for different directions, crystallite sizes along [1 1 0] and [0 1 5] become almost same after 5h of milling (~17.5 nm) and this value is slightly higher than that of along [1 0 10] (~15.1 nm). This trend in crystallite size variation continues to the end of milling. The saturation crystallite size value is ~17 nm along [1 1 0] and [0 1 5], whereas ~15 nm along [1 0 10].

The variation of r.m.s. lattice strain of Bi₂Te₃ is plotted in Fig. 5 and the lattice strain values are also different in different crystallographic directions. Similar to crystallite size variation, after 5h milling r.m.s. lattice strain along [1 1 0] releases to a large extent and become nearly equal to that along [0 1 5]. Whereas, r.m.s. lattice strain along [1 0 10] increases after 5h of milling and even after 10 h of milling strain along [1 0 10] remains higher than along [0 1 5] or [1 1 0]. Analyzing the nature of variation of crystallite size and r.m.s. lattice strain value along with the directions considering three major reflections, it is evident that the mechanically synthesized Bi₂Te₃ nanocrystals are anisotropic in nature. However, higher time of milling after 5h results in a large impact by reducing the level of anisotropy of both crystallite size and lattice strain.

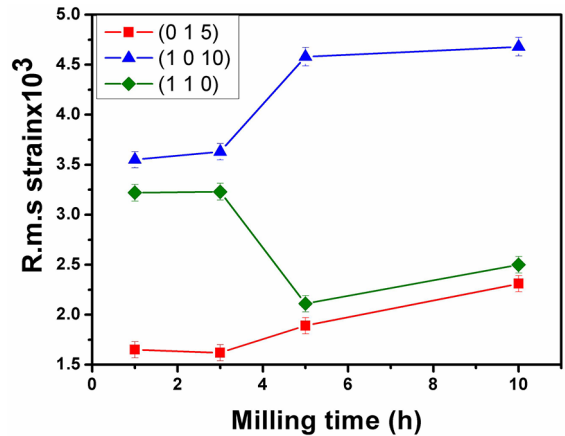


Figure 5. Variation of r.m.s. strains of Bi₂Te₃ phase with increasing milling time.

The HRTEM images of 10 h ball-milled powder are shown in Figs. 6(a)-(d). Miller indices of different crystal planes shown in the indexed selected area electron diffraction (SAED) pattern of Fig. 6(a) clearly reveals that the 10 h milled sample contains only the Bi₂Te₃ reflections.

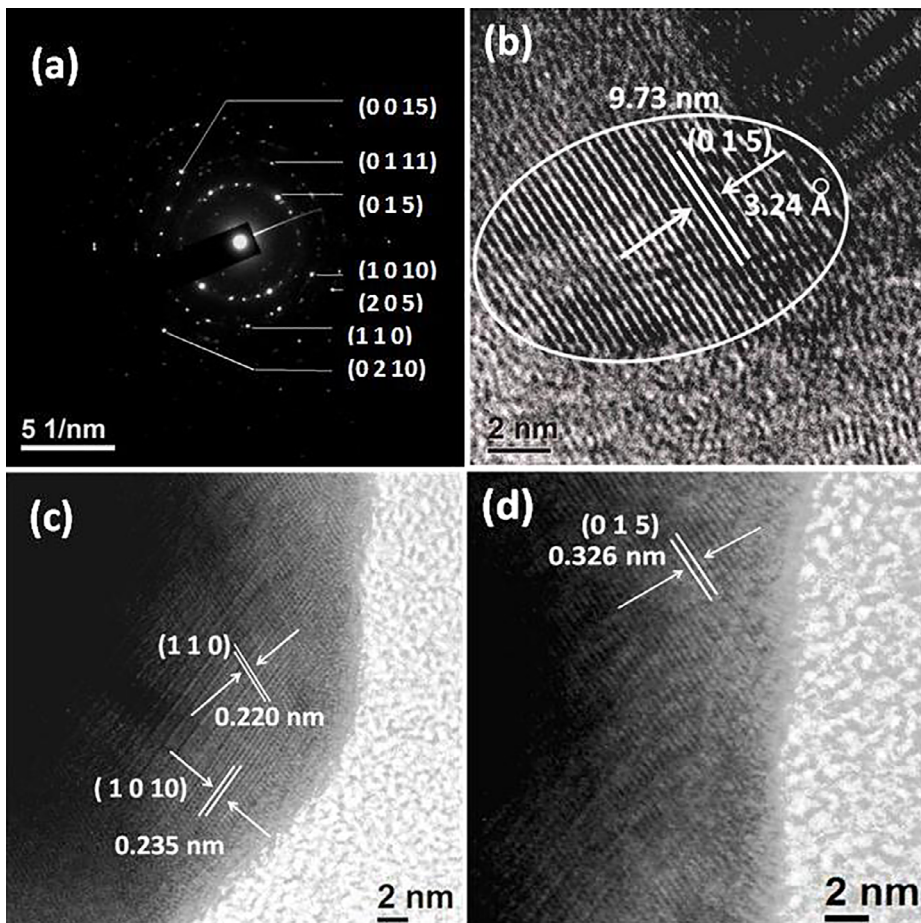


Figure 6. (a) Indexed selected area electron diffraction (SAED) pattern of 10h ball-milled Bi₂Te₃ powders (b). Brightfield TEM image of 10h ball-milled powder containing Bi₂Te₃ nanoparticle (marked by white ring) (c) & (d) HRTEM micrograph revealing (110), (1010) and (015) planes of nanocrystalline Bi₂Te₃ in 10h ball-milled powder mixture.

An isolated Bi_2Te_3 nanoparticle (marked by white ring) as shown in the HRTEM image of Fig. 6(b) is clearly anisotropic in nature with average particle size ~ 9.73 nm which is smaller than the crystallite size obtained from Rietveld analysis of XRD pattern. The interplanar spacing of the planes of a nanocrystalline particle is calculated from Fig. 6(b) and the value 0.324 nm corresponds to the densest (0 1 5) plane of Bi_2Te_3 lattice. Crystal planes with different orientations have also been clearly noticed in both Figs. 6(c) and (d) and the calculated interplanar spacing shown in the figures in each case gives direct evidence of the full formation of the trigonal Bi_2Te_3 phase in 10 h milled sample.

4.2 Electrical conductivities of ball milled samples measured at different temperatures

In this present study, DC electrical conductivities of 15min, 30min and 10h ball milled Bi_2Te_3 samples have been measured within the temperature range of 359 to 633K. It is to be noted that both 15min and 30min ball milled samples are composed of major Bi_2Te_3 phase and two minor BiTe phases and the 10h milled sample contains only the Bi_2Te_3 phase.

The conductivity ratio, $\sigma_r [\sigma(633\text{K})/\sigma(359\text{K})]$ is approximately equal to 2.6364 for 10h milled sample. In Fig. 7 (a), variations of DC resistances with temperature of these samples are plotted. It is evident that after 15min of milling, the increase of DC resistance with temperature dominates the metallic behaviour of the sample. After 30min of milling, a significant change is noticed. In the lower temperature range up to $\sim 423\text{K}$, the DC resistance shows the metallic and semiconducting behaviours and after that, it shows completely semiconducting behavior up to 633K with increasing DC conductivity with temperature. However, after 10h milling when there is no trace of minor BiTe phases (Table 2), DC resistance decreases significantly by factor ~ 10 and the sample shows the semiconducting nature in the entire range of measuring temperature. These nature of electrical behaviors can be interpreted by the following manners: (a) the metallic nature of 15h milled sample is due to the presence of two significant amount (Table 2) of two minor BiTe phases, (b) presence of minor BiTe phases in 30min milled sample is insignificant (Table 2) and the metallic behaviour at low-temperature range may be due

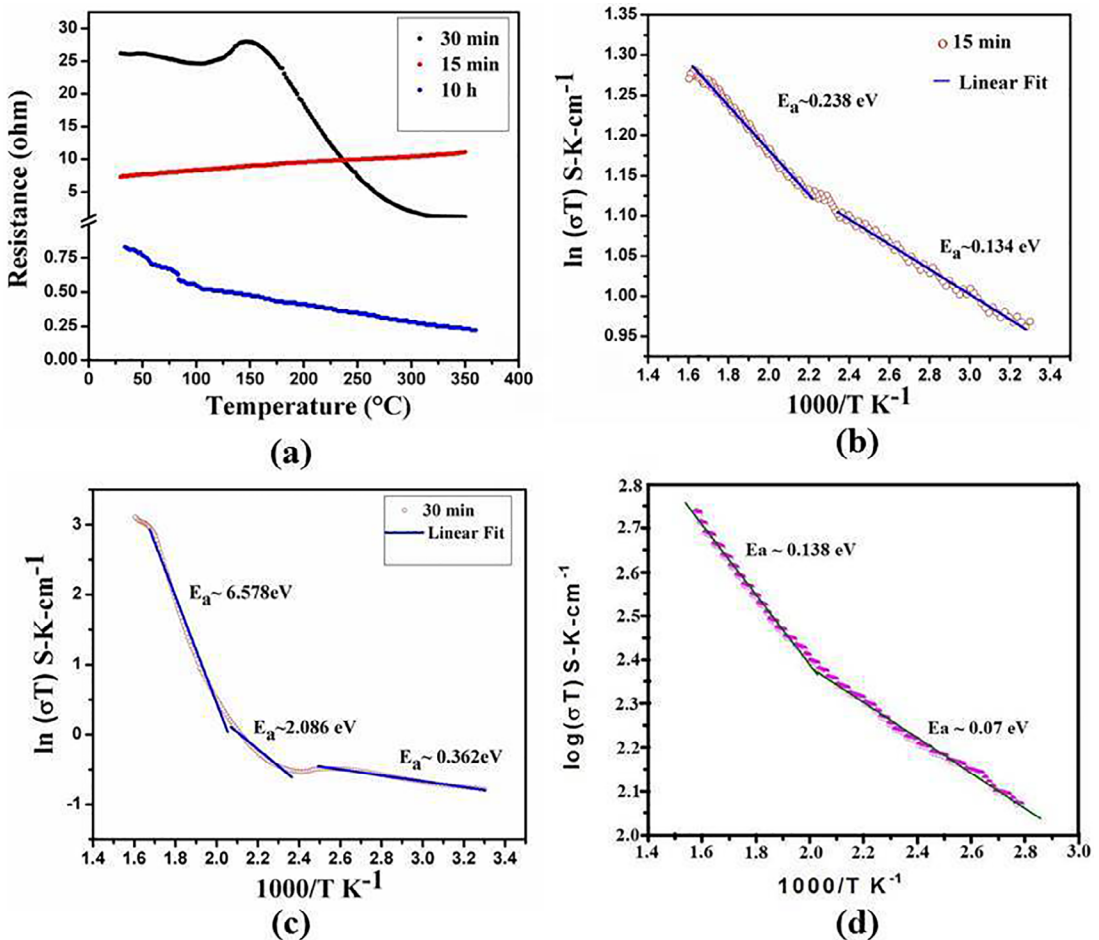


Figure 7. (a) Variation of DC resistance of 15min, 30min and 10h milled samples with temperature (b) Activation energies of 15min ball milled sample at different temperature regions (c) Activation energies of 30 min ball milled sample at different temperature regions (d) Plot of $\log \sigma T$ with $1000/T$ after measurement the DC electrical conductivity of 10h ball-milled Bi_2Te_3 .

these phases and at elevated temperatures, these phases seem to dissolve in major Bi₂Te₃ phase and after that the single stoichiometric Bi₂Te₃ phase shows semiconducting behaviour, (c) after 10h of milling the stoichiometric Bi₂Te₃ has been formed and the conductivity of the semiconducting sample increases significantly due to the absence of these minor metallic BiTe phases. The variations of $\log(\sigma T)$ (S-cm⁻¹) with $1000/T$ (K⁻¹) for 15min, 30min and 10h milled samples are plotted in Figs. 7(b), (c) and (d) respectively. From these figures, it is clear that $\log(\sigma T)$ and consequently the electrical conductivities (σ) of these samples are increasing with temperature indicating more or less the semiconducting nature of the samples. This type of variation can be explained by the tunnelling type conduction model and according to this model the electrical conductivity σ_T is given by^{31,32}

$$\sigma_T \propto \exp[-2kt - E_c/(2K_B T)] \quad (1)$$

where the tunnel barrier thickness is denoted by t , barrier parameter is denoted by k and E_c is the charging energy. This charging energy E_c is related with activation energy E_a by the relation $E_c = 2E_a$. For uniform barrier thickness, eq. (1) can be simplified as³¹,

$$\sigma_T \propto \exp[-E_a/(K_B T)] \quad (2)$$

The rate of change of $\log(\sigma T)$ with temperature is different for low and high-temperature regions. So, at least two different values of activation energies (E_a) are obtained for all three samples. In the case of the 10h milled sample, $E_a = 0.07$ eV and 0.138 eV are obtained for lower and higher temperature region respectively. In 2010, Pradyumnan et al.³³ reported the values of activation energy of unannealed and annealed Bi₂Te₃ samples as 0.005 eV and 0.016 eV respectively. Activation energies of Bi₂Te₃ thin films were found to be 0.0426 eV, 0.0386 eV, 0.0333 eV and 0.0277 eV for different thickness of the film³⁴. In 2017, Vinoth et al. reported the value of activation energy of Bi₂Te₃ as 0.042 eV estimated from the Arrhenius plot³⁵. Thus, the activation energy of the nanocrystalline Bi₂Te₃ sample synthesized by mechanical alloying is very close to the reported values.

Relatively high activation energy at higher temperature indicates that more and more immobile charge carriers have become mobile with the increasing temperature which leads to an increase in electrical conductivity (σ) of all three samples at elevated temperatures. It, therefore, indicates that the DC resistance behaviour of the 15min milled sample is a mixture of metallic and semiconducting compounds, though it shows the metallic character. It may be noted that the value of conductivity of the 10h milled sample is not very high due to the possibility of having a large amount of porosity in the pellets made from ball-milled nano-dimensional powders that result in a reduction of electrical conductivity.

However, there is no noticeable change in electrical conductivities of Bi₂Te₃ phase since its formation after 15min till the end of milling up to 10h, as there is no significant change in crystallite size of the phase with increasing milling time.

5. Conclusions

In the present study, nanocrystalline Bi₂Te₃ powder has been synthesized by mechanical alloying the stoichiometric powder mixture of Bi and Te powders under Ar in a short time of 15 min with two structurally unknown minor phases. Structure models of these two new phases have been proposed for the first time. Full formation of Bi₂Te₃ has been achieved after 1h of milling. Microstructure characterization by Rietveld analysis reveals both crystallite size and r.m.s. lattice strain are anisotropic in nature. HRTEM images of 10 h milled powder mixture confirm the formation of stoichiometric nanocrystalline Bi₂Te₃ phase. The DC electrical conductivities of the 15min, 30min and 10 h ball-milled samples with increasing temperature clearly reveals the metallic nature of the 15min sample and semiconducting nature of 30min and 10h milled samples. However, there is no significant change in electrical conductivities of Bi₂Te₃ phase since its formation after 15min till the end of milling up to 10h.

6. Acknowledgements

One of the authors S.K.P. wishes to thank the University Grants Commission for granting the Major Research Project [F. No. 41-845/2012(SR)] to the University of Burdwan under the financial assistance of which the work has been carried out. One of the authors TC is grateful to the Department of Science and Technology (DST), Govt. of India for INSPIRE fellowship (IF-160606).

7. References

- Vineis CJ, Shakouri A, Majumdar A, Kanatzidis MG. Nanostructured Thermoelectrics: Big Efficiency Gains from small features. *Advanced Materials*. 2010 Sep;22(36):3970-3980.
- Bell LE. Cooling, heating, generating power and recovering waste heat with thermoelectric systems. *Science*. 2008 Sep;321(5895):1457-1461.
- Goldsmid HJ. *Thermoelectric Refrigeration*. New York: Plenum Press; 1964.
- Yim WM, Rosi FD. Compound tellurides and their alloys for peltier cooling – a review. *Solid-State Electron*. 1972 Oct;15(10):1121-1140.
- Rowe DM. *CRC Handbook of Thermoelectrics*. New York: CRC Press Inc.; 1995.
- Snyder GJ, Toberer ES. Complex thermoelectric materials. *Nature Materials*. 2008 Feb;7:105-114.
- Liu W, Yan X, Chen G, Ren Z. Recent advances in thermoelectric nanocomposites. *Nano Energy*. 2012 Jan;1(1):42-56.

8. Poudeu PF, D'Angelo J, Kong HJ, et al. Nanostructures versus solid solutions: low lattice thermal conductivity and enhanced thermoelectric figure of merit in $\text{Pb}_{9.6}\text{Sb}_{0.2}\text{Te}_{10-x}\text{Sex}$ bulk materials. *Journal of the American Chemical Society*. 2006 Nov;128(44):14347-55.
9. Poudeu PFP, Guéguen A, Wu CI, Hogan T, Kanatzidis MG. High Figure of Merit in Nanostructured n-Type $\text{KPB}_m\text{SbTe}_{m+2}$ Thermoelectric Materials. *Chemistry of Materials*. 2010 Sep;22(3):1046-1053.
10. Zakeri M, Allahkarami M, Kavei Gh, Khanmohammadian A, Rahimpour MR. Synthesis of nanocrystalline Bi_2Te_3 via mechanical alloying. *Journal of Materials Processing Technology*. 2009;209:96-101.
11. Yang J, Aizawa T, Yamamoto A, Ohta T. Effect of processing parameters on thermoelectric properties of p-type $(\text{Bi}_2\text{Te}_3)_{0.25}(\text{Sb}_2\text{Te}_3)_{0.75}$ prepared via BMA-HP Method. *Materials Chemistry and Physics*. 2001;70(1):90-94.
12. Kim HC, Oh TS, Hyun DB. Thermoelectric properties of the p-type $\text{Bi}_2\text{Te}_3\text{-Sb}_2\text{Te}_3\text{-Sb}_2\text{Se}_3$ alloys fabricated by mechanical alloying and hot pressing. *Journal of Physics and Chemistry of Solids*. 2000 Mar;61(5):743-749.
13. Yu F, Zhang J, Yu D, He J, Liu Z, Xu B, Tian Y. Enhanced thermoelectric figure of merit in nanocrystalline Bi_2Te_3 bulk. *Journal of Applied Physics*. 2009 May;105:094303.
14. Jimenez S, Perez JG, Tritt TM, Zhu S, Sosa-Sanchez JL, Martinez-Juarez J, López O. Synthesis and thermoelectric performance of a p-type $\text{Bi}_{0.4}\text{Sb}_{1.6}\text{Te}_3$ material developed via mechanical alloying. *Energy Conversion and Management*. 2014;87:868-873.
15. Einaga M, Ohmura A, Nakayama A, Ishikawa F, Yamada Y, Nakano S. Pressure induced phase transition of Bi_2Te_3 to a bcc structure. *Physical Review B*. 2011 Mar;83(9):1-4.
16. Nakayama A, Einaga M, Tanabe Y, Nakano S, Ishikawa F, Yamada Y. Structural phase transition in Bi_2Te_3 under high pressure. *High Pressure Research*. 2009 May;29(2):245-249.
17. Humphry-Baker SA, Schuh CA. The nanocrystalline thermoelectric compound Bi_2Te_3 forms by a particle-wise explosive reaction during mechanical alloying. *Scripta Materialia*. 2011;65:516-519.
18. Dutta H, Sahu P, Pradhan SK, De M. Microstructure characterization of polymorphic transformed ball-milled anatase TiO_2 by Rietveld method. *Materials Chemistry and Physics*. 2002;77:153-164.
19. Manik SK, Dutta H, Pradhan SK. Microstructure characterization and phase transformation kinetics of polymorphic transformed ball milled a-TiO₂-10 mol% m-ZrO₂ mixture by Rietveld method. *Materials Chemistry and Physics*. 2003 Dec;82(3):848-859.
20. Lutterotti L, MAUD version 2.79. <http://maud.radiographema.eu>
21. Lutterotti L, Scardi P, Maistrelli P. LSI – A computer program for simultaneous refinement of material structure and microstructure. *Journal of Applied Crystallography*. 1992;25:459-462.
22. Rietveld HM. Line profiles of neutron powder-diffraction peaks for structure refinement. *Acta Crystallographica*. 1967;22(1):151-152.
23. Rietveld HM. A profile refinement method for nuclear and magnetic structures. *Journal of Applied Crystallography*. 1969;2:65-71.
24. Young RA, Wiles DB. Profile shape functions in Rietveld refinements. *Journal of Applied Crystallography*. 1982;15:430-438.
25. Sinha M, Dutta H, Pradhan SK. Phase stability of nanocrystalline Mg-Zn ferrite at elevated temperatures. *Japanese Journal of Applied Physics*. 2008 Nov;47(11):8667-8672.
26. Toraya H. Estimation of statistical uncertainties in quantitative phase analysis using the Rietveld method and the whole-powder-pattern decomposition method. *Journal of Applied Crystallography*. 2000 Dec;33(6):1324-1328.
27. Dutta H, Nandy A, Pradhan SK. Microstructure and optical characterizations of mechano-synthesized nanocrystalline semiconducting ZrTiO_4 compound. *Journal of Physics and Chemistry of Solids*. 2016;95:56-64.
28. Nandy A, Dutta A, Pradhan SK. Microstructure correlated electrical conductivity of Manganese alloyed nanocrystalline cubic zirconia synthesized by mechanical alloying. *Advanced Powder Technology*. 2017;28(2):618-628.
29. Dutta H, Bandyopadhyay S, Sain S, Pradhan SK. Microstructure characterization of intermetallic $(\text{Ni-Ti})_3\text{C}$ nanocarbide compound synthesized by mechanical alloying of elemental powders. *Ceramics International*. 2018;44(12):14857-14864.
30. Gajović A, Tomasić N, Djerđić I, Su DS, Furić K. Influence of mechanochemical processing to luminescence properties in Y_2O_3 powder. *Journal of Alloys and Compounds*. 2008 May;456(1-2):313-319.
31. Neugebauer CA, Webb MB. Electrical conduction mechanism in ultrathin, evaporated metal films. *Journal of Applied Physics*. 1962;33:74-82.
32. Sheng P, Abeles B, Arie Y. Hopping conductivity in granular metals. *Physical Review Letters*. 1973 Jul;31(1):44-47.
33. Pradyumn PP, Swathikrishnan. Thermoelectric properties of Bi_2Te_3 and Sb_2Te_3 and its bilayer thin films. *Indian Journal of Pure and Applied Physics*. 2010 Feb;48:115-120.
34. Zeng Z, Yanga P, Hu Z. Temperature and size effects on electrical properties and thermoelectric power of Bismuth Telluride thin films deposited by co-sputtering. *Applied Surface Science*. 2013;268:472-476.
35. Vinoth S, Balaganapathi T, KaniAmuthan B, Arun T, Muthuselvam IP, Chou FC, Thilakan P. Bi_2Te_3 thin hexagonal nanoplatelets: Synthesis and its characterization studies. *Physica E: Low-dimensional Systems and Nanostructures*. 2017;92:17-22.